

Numerical Study on Waste Heat Recovery Characteristics of Non-Newtonian Thermally Hydrolyzed Sewage Sludge Using Dimpled Tubes

Songning Xiong^a, Zhigen Wu^{b,c}, Wei Lu^{a,*}, Yanping Du^d, Guanhua Zhang^a, Zhibo Xiong^a
Yupeng Wu^e

^a School of Energy and Power Engineering, University of Shanghai for Science and Technology, Shanghai, 200093, China

^b State Key Laboratory of Pollution Control and Resource Reuse, College of Environmental Science and Engineering, Tongji University, Shanghai, 200092, China

^c Shanghai Institute of Pollution Control and Ecological Security, China

^d School of Engineering, Lancaster University, Lancaster LA1 4YW, UK

^e Faculty of Engineering, University of Nottingham, Nottingham NG7 2RD, UK

* Corresponding author. Email: wei.lu@usst.edu.cn.

Abstract: Following high-temperature thermal hydrolysis treatment, the sewage sludge contains substantial quantities of recoverable waste heat. Enhancing the waste heat recovery efficiency from this thermally hydrolyzed sludge can significantly reduce the operational costs of wastewater treatment plants. This study investigates the performance and entropy generation characteristics of waste heat recovery from thermally hydrolyzed sewage sludge with non-Newtonian fluid properties using dimpled tubes through numerical simulations. The experimental results demonstrate that dimpled tubes exhibit superior waste heat recovery efficiency compared to smooth tubes. Overall, the ellipsoidal dimpled tubes exhibit superior Performance Evaluation Criteria (*PEC*) values compared to spherical configurations, whereas spherical dimpled tubes demonstrate better entropy production performance. Specifically, under the same geometric parameters, the Nusselt number (*Nu*) and friction factor (*f*) of ellipsoidal dimpled tubes are 1.63-1.92 times and 2.65-3.32 times of smooth tubes, respectively, with a maximum *PEC* value of 1.39. Under the same geometric parameters compared to smooth tubes, the entropy generation is reduced by up to 50% for spherical dimpled tubes. Furthermore, the results indicate that the relative influence of dimple geometric parameters on various performances exhibits a hierarchy of depth > number > pitch. These results provide valuable insights into the complex interplay between geometric parameters and non-Newtonian fluid flow characteristics.

Keywords: thermal-hydraulic performance, dimpled tube, entropy production, thermally hydrolyzed sewage sludge, non-Newtonian fluid, waste heat recovery

Nomenclature		<i>Re</i>	Reynolds number
<i>a</i>	Dimple width (mm)	<i>S_{gen}</i>	Total entropy production rate (W/K)
<i>b</i>	Dimple major axis length (mm)	<i>S_{gent}</i>	Thermal entropy production rate (W/K)

Be	Bejan number	$S_{gen,f}$	Friction entropy production rate (W/K)
c_p	specific heat capacity (J/kgK)	T	Temperature (K)
d	Dimple diameter	u	Velocity (m/s)
D	Dimple depth mm	V	Volume of the fluid domain
D_h	Hydraulic diameter mm		
f	Friction factor	Greek symbols	
h_i	Convective heat transfer coefficient (W/m ² K)	ρ	Density (kg/m ³)
J_{ABS}^n	Secondary flow intensity (s ⁻¹)	μ	Dynamic viscosity (Pa·s)
k	Turbulent kinetic energy (m ² /s ²)	μ_t	Turbulent viscosity (Pa·s)
K	consistency index (Pa·s)	ε	Dissipation rate of turbulence (m ² /s ³)
L	Length mm	Γ	Generalized diffusion coefficient
m	Mass flow rate (kg/s)	λ	The thermal conductivity (W/mK)
n	power law index	τ	Apparent viscosity (Pa·s)
N	Dimple number	γ	Shear rate (s ⁻¹)
Nu	Nusselt number	σ_k	Prandtl number for k
N_s	Enhanced entropy production ratio	σ_ε	Prandtl number for ε
p	Pressure (Pa)	ω^i	Component of vorticity
P	Dimple pitch (mm)	Δ	Difference
PEC	Performance evaluation criterion		
Pr	Prandtl number	Subscripts	
Pr_t	Turbulent Prandtl number.	b	bulk
q	Heat transfer rate per unit length flux (W/m)	s	Smooth tube
q''	Heat flux (W/m ²)	w	Tube wall
Q	Total heat (J)		

1. Introduction

Wastewater represents a critical environmental concern, with its annual generation volume persistently rising. Sewage sludge, as an unavoidable byproduct of wastewater treatment processes, contains substantial amounts of toxic components including heavy metals and pathogenic microorganisms. Improper utilization or disposal of such sludge consequently endangers both public health and ecological systems [1].

Anaerobic digestion represents a viable sludge treatment approach that simultaneously generates bioenergy products (methane/hydrogen), mitigates greenhouse gas emissions, and controls odor generation while reducing pathogenic microorganisms [2, 3]. Nevertheless, the intricate floc structure and recalcitrant cellular membranes of microbial constituents in sewage sludge compromise the hydrolytic efficacy of anaerobic digestion processes, thereby impeding the bioconversion of organic substrates into methane [4]. Therefore, pretreatment of sewage sludge is necessary before anaerobic digestion.

Among diverse pretreatment approaches, thermal hydrolysis technology enhances process kinetics and methane yield in anaerobic digestion systems, while concurrently delivering multiple operational advantages including augmented biosolid dewaterability, pathogen inactivation, and rheological modification of digestates [5, 6]. In addition, because the management and treatment of sewage sludge is costly, accounting for almost about half of the total operating costs of sewage treatment plants. The application of thermal hydrolysis technology requires injecting a significant amount of heat into the sewage sludge to reach the specified thermal hydrolysis temperature. The use of heat exchangers allows effective recovery and reuse of process thermal energy, thereby enhancing energy efficiency and lowering operational costs in sludge treatment [7-9].

Thermal hydrolysis technology can be classified into high-temperature ($>100^{\circ}\text{C}$) and low-temperature ($<100^{\circ}\text{C}$) processes based on operating conditions [10]. Since the optimal temperature for anaerobic digestion is $30\text{-}55^{\circ}\text{C}$ and the sewage sludge undergoing high-temperature thermal hydrolysis retains substantial recoverable thermal energy [11], thermally hydrolyzed sewage sludge requires sufficient cooling prior to introduction into anaerobic digestion systems. During this process, the use of a heat exchanger can effectively cool the sewage sludge while also recovering heat. Among various types of heat exchangers, tube heat exchangers are suitable for cooling or heating high viscosity and corrosive fluids such as sewage sludge due to the simple manufacturing, strong compression resistance and corrosion resistance [12].

As essential heat transfer equipment in industrial applications, improving the heat transfer efficiency of heat exchangers is crucial for achieving compact designs and performance optimization. To enhance heat transfer efficiency, researchers have developed three primary enhancement methods: active, passive and hybrid techniques. Passive methods are particularly advantageous in practical implementations due to the absence of external energy requirements [14], helically grooved tubes [15], corrugated tubes [16] and tube inserts such as twisted tapes [17] and coils [18] is the most common passive heat transfer enhancement techniques. Dimpled tubes, with their advantages of easy processing, effective enhancement of heat transfer performance, and smaller resistance increase, are particularly suitable for flow heat transfer processes involving high-viscosity and highly corrosive fluids such as sewage sludge [19-21].

The thermohydraulic characteristics of dimpled tubes are governed by key structure parameters, including dimple shape, depth, pitch, etc. Wang et al. [22] experimentally studied the airflow and

heat transfer behavior in dimpled tubes with spherical and ellipsoidal dimples. Their results demonstrated that both dimple configurations enhanced heat transfer coefficients and increased resistance compared to smooth tubes. Notably, ellipsoidal dimpled tubes achieved higher thermal performance with lower flow resistance than spherical dimpled tubes. Li et al. [23] examined the thermal-fluid dynamics of water flow within dimpled tubes with ellipsoidal, spherical, and conical dimples. Experimental results demonstrated that ellipsoidal dimple configurations exhibited enhanced overall thermal efficiency compared to spherical and conical geometries under equivalent flow conditions. Sabir et al. [24] conducted a numerical investigation using water as the working fluid to evaluate the thermal-hydraulic performance of dimpled tubes by varying both the number of dimples and their deflection angles. Their results demonstrated that ellipsoidal dimpled tubes with a 0° deflection angle achieved optimal performance under higher Reynolds number conditions, while a 45° deflection angle was more effective at lower Reynolds numbers. Furthermore, configurations with six transversely arranged dimples exhibited the highest heat transfer efficiency. Zhang et al. [25] numerically investigated to evaluate the thermohydraulic performance of dimpled tubes with cross-combined elliptical dimples. Their analysis revealed that these cross-combined elliptical dimple configurations demonstrated higher performance evaluation criterion values compared to conventional single-ellipsoid dimpled tubes.

Vicente et al. [26] investigated the flow and heat transfer of water and ethylene glycol within helically dimpled tubes, focusing on the effects of dimple depth and pitch. Aroonrat et al. [27] examined the role of dimple depth variations in modulating phase-change heat transfer characteristics for R-134a refrigerant flowing through dimpled tubes. Gürsoy et al. [28-30] investigated the thermo-hydraulic performance and entropy generation characteristics of nanofluids in sudden expanded tube with dimples and bended dimpled tube. Pazarlıoğlu et al. [31] investigated the thermo-hydraulic performance and entropy generation characteristics of nanofluids in sudden expanded tube with elliptical dimples. Kaood et al. [32] investigated hydrothermal and entropy generation performance of convergent tubes with various dimple shapes.

Totally, the working fluid used is almost Newtonian fluid in these studies. There is few research on the thermo-hydraulic performance of non-Newtonian fluids in dimpled tubes, and lack of the analysis on enhanced heat transfer mechanism. Thermal hydrolyzed sewage sludge, a characteristic non-Newtonian fluid, serves as the working medium in this numerical investigation of

thermohydraulic behavior and entropy generation within dimpled tubes. Parametric analyses systematically evaluate the effects of dimple geometry (shape, depth), spatial arrangement (pitch, transverse density), and flow conditions ($Re = 3000\sim 8000$) on thermo-hydraulic performance and entropy production. This study aims to enhance the efficiency of thermally hydrolyzed sewage sludge waste heat recovery systems while extending the applicability of dimpled tube.

2. Numerical model

2.1. Physical model

The dimpled tubes employed in this investigation are illustrated in Fig. 1, featuring a diameter $d = 25\text{mm}$. The dimples are uniformly distributed along the tube's circumference at identical intervals. Key investigated parameters include dimple geometry, depth D , pitch P , and transverse dimple count N . All dimples maintain a constant width $a = 4\text{ mm}$, with elliptical configurations additionally specifying a major axis length $b = 6\text{ mm}$. Table 1 comprehensively documents the dimensional and configurational parameters for all simulated configurations.

Table 1
Geometric defining parameters of dimples.

	Shape	D (mm)	N	P (mm)
Case A	Ellipsoidal, Spherical, Conical	2.0	8	13
Case B	Ellipsoidal	1.5, 2.0, 2.5	8	13
Case C	Ellipsoidal	2.0	4, 6, 8	13
Case D	Ellipsoidal	2.0	8	13, 19, 25

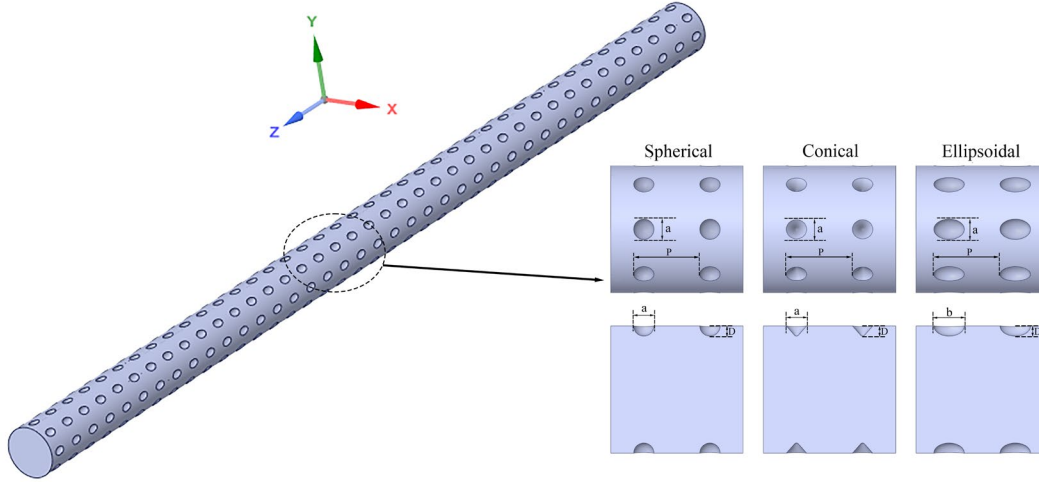


Fig. 1. Schematic illustration of dimpled tubes with varying dimple geometries.

2.2. Governing equation

Fluid flow and heat transfer are governed by the incompressible mass, momentum, and energy conservation equations. Steady-state simulations were conducted using the Reynolds-Averaged Navier-Stokes (RANS) framework, with the Realizable $k-\varepsilon$ (RKE) turbulence model adopted to close the RANS equations. In the study of Liao et al.[33], the Realizable $k-\varepsilon$ turbulence model yielded optimal results. And in the study of Lin et al.[34], the model demonstrated its applicability in the field of shear thinning non-Newtonian fluids. The associated governing equations are as follows:

Continuity equation [34]:

$$\frac{\partial}{\partial x_i}(\rho u_i) = 0 \quad (1)$$

Momentum equation [34]:

$$\frac{\partial}{\partial x_j}(\rho u_i u_j) = -\frac{\partial p}{\partial x_i} + \frac{\partial}{\partial x_j}(\mu + \mu_t) \left(\frac{\partial u_j}{\partial x_i} + \frac{\partial u_i}{\partial x_j} \right) \quad (2)$$

Energy equation [34]:

$$\frac{\partial}{\partial x_i}(u_i T) = \frac{\partial}{\partial x_i} \left[\left(\frac{\mu}{Pr} + \frac{\mu_t}{Pr_t} \right) \frac{\partial T}{\partial x_i} \right] \quad (3)$$

where ρ is fluid density, u is velocity, p is pressure, μ is dynamic viscosity, μ_t is turbulent viscosity, T is temperature, Pr is the Prandtl number, Pr_t is turbulent Prandtl number.

Turbulence kinetic energy (k) equation [34]:

$$\frac{\partial}{\partial x_j}(\rho k u_j) = \frac{\partial}{\partial x_j} \left[\left(\mu + \frac{\mu_t}{\sigma_k} \right) \frac{\partial k}{\partial x_j} \right] + \Gamma - \rho \varepsilon \quad (4)$$

Dissipation rate of turbulence (ε) equation [34]:

$$\frac{\partial}{\partial x_j}(\rho \varepsilon u_j) = \frac{\partial}{\partial x_j} \left[\left(\mu + \frac{\mu_t}{\sigma_\varepsilon} \right) \frac{\partial \varepsilon}{\partial x_j} \right] + C_1 \Gamma \varepsilon - C_2 \frac{\varepsilon^2}{k + \sqrt{\nu \varepsilon}} \quad (5)$$

where Γ can be expressed as [34]:

$$\Gamma = -\overline{u_i u_j} \frac{\partial u_i}{\partial u_j} = \frac{\mu_t}{\rho} \left(\frac{\partial u_i}{\partial x_j} + \frac{\partial u_j}{\partial x_i} \right) \frac{\partial u_i}{\partial x_j} \quad (6)$$

$$\mu_t = \rho C_\mu \frac{k^2}{\varepsilon} \quad (7)$$

The constants of the realizable k - ε equations are given as below [34]:

$$C_1 = \max \left[0.43, \frac{\mu_t}{\mu_t + 5} \right], C_2 = 1.0, \sigma_k = 1.0, \sigma_\varepsilon = 1.2 \quad (8)$$

2.3. Properties of working fluid

The working fluid used in this study is thermal-hydrolyzed sewage sludge with a solid content of 1.2%. Which exhibits the power-law rheological behavior expressed as [35]:

$$\tau = K (\dot{\gamma})^n \quad (9)$$

where $\dot{\gamma}$ is shear rate, n is power law index and K is consistency index. In this study, $n=0.71$ and $K=0.02$ (Pa·s) [35].

Given the relatively low solids content and the effective dissolution of larger particulate matter through high-temperature thermal hydrolysis in sewage sludge, interparticle forces are considered negligible, permitting the assumption of single-phase flow behavior. This hypothesis can be confirmed by the research of Chen et al [36]. The thermal conductivity $\lambda = 0.7$ (W/mK), density $\rho = 1004$ (kg/m³), specific heat capacity $c_p = 4200$ (J/kgK).

2.4. Boundary conditions

Owing to the periodic distribution of dimples along the tube surface, periodic boundary

conditions were applied in this study. This approach ensures hydrodynamic fully developed flow while significantly reducing computational costs. The mathematical formulation of the periodic boundary conditions is defined as follows [37]:

$$u_x(x, y, 0) = u(x, y, L), u_y(x, y, 0) = u(x, y, L), u_z(x, y, 0) = \frac{m_{test}}{m_{out}} w(x, y, L) \quad (10)$$

$$k(x, y, 0) = k(x, y, L), \varepsilon(x, y, 0) = \varepsilon(x, y, L) \quad (11)$$

$$T(x, y, 0) = T(x, y, L) - \frac{Q}{c_p m_{out}} \quad (12)$$

where Q is the total heat absorbed by heat transfer fluid, c_p is specific heat capacity, L is the length of test section, m is mass flow rate and its value is calculated according to the given Re .

Wall boundary conditions:

$$Q = Q_w = const, u_x = u_y = u_z = 0 \quad (13)$$

The implementation of periodic boundary conditions results in minimal temperature variation within a single periodic unit, permitting the assumption of temperature-independent thermophysical properties for the fluid. And this hypothesis has also been confirmed in the research of Xie et al [37].

Initial fluid temperature was fixed at 370 K, with $Re = 3,000\text{--}8,000$ to replicate operational conditions of practical heat exchangers. No-slip boundary conditions and a constant uniform heat flux $q'' = -50\text{kW/m}^2$ were imposed on the tube wall surface.

2.5. Numerical method

Numerical simulations were conducted using ANSYS Fluent, employing the Finite Volume Method to solve the governing equations. The SIMPLE algorithm resolved velocity-pressure coupling, while second-order upwind schemes discretized convective and diffusive terms. Convergence criteria required residuals below 10^{-8} for the energy equation and 10^{-5} for other variables, supplemented by stabilized monitoring of Nusselt number and friction factor.

2.6. Evaluating indicator

For non-Newtonian fluids, the generalized Reynolds number proposed by Metzner Reid is used.

The Metzner-Reid Reynolds number (Re) is defined as [38]:

$$Re = \frac{\rho u^{2-n} D_h^n}{8^{n-1} K \left(\frac{3n+1}{4n} \right)^n} \quad (14)$$

where D_h is hydraulic diameter, which is considered equal to the geometric diameter in this study and the values of n and K are provided in Section 2.3.

The Prandtl number (Pr) is defined as [38]:

$$Pr = \frac{c_p K (u / D_h)^{n-1}}{\lambda} \quad (15)$$

The convective heat transfer coefficient (h_i) is defined as [25]:

$$h_i = \frac{q}{T_b - T_w} \quad (16)$$

where T_b is the mass-weighted average temperature of the fluid and T_w is the area-weighted average temperature of tube wall.

The average Nusselt number (Nu) is defined as [25]:

$$Nu = \frac{h_i D_h}{\lambda} \quad (17)$$

The friction factor (f) is defined as [25]:

$$f = \frac{2\Delta p D_h}{\rho u^2 L} \quad (18)$$

where Δp is the pressure drop of the test section.

The overall thermo-hydraulic performance of the enhanced tube was quantitatively assessed using the performance evaluation criterion (PEC), defined as [25]:

$$PEC = \frac{Nu / Nu_0}{(f / f_0)^{1/3}} \quad (19)$$

where Nu_0 and f_0 denote Nusselt number and friction factor for smooth tube, respectively.

Entropy generation within the system arises from thermodynamic irreversibility, including chemical reactions, viscous friction, and finite temperature gradients. Minimizing entropy production reflects decreased inherent irreversibility in flow and heat transfer mechanisms, thereby enhancing energy conversion efficiency through reduced dissipative losses. The total entropy production rate (S_{gen}) is obtained as [39]:

$$S_{gen} = S_{gen,t} + S_{gen,f} \quad (20)$$

where $S_{gen,t}$ is the thermal entropy production rate, can be calculated with Eq. (21) [40]. $S_{gen,f}$ is the friction entropy production rate, can be calculated with Eq. (22) [40].

$$S_{gen,t} = \frac{q^2 D_h^2 \pi L}{Nu \lambda T_b^2} \quad (21)$$

$$S_{gen,f} = \frac{32 m^3 f L}{\pi^2 D_h^5 \rho^2 T_b} \quad (22)$$

The Bejan number (Be) quantifies the relative contribution of thermal entropy to total entropy production. The closer the value of Be is to 1, the greater the contribution of thermal entropy to the total entropy, which is more conducive to the heat transfer process. It is expressed as [39]:

$$Be = \frac{S_{gen,t}}{S_{gen}} \quad (23)$$

The enhanced entropy production ratio, N_s can be calculated with Eq. (24) [40]. When $N_s < 1$ It indicates that the opted enhancement method is conducive to reducing the irreversibility of the heat transfer while enhancing it.

$$N_s = \frac{S_{gen}}{S_{gen,s}} \quad (24)$$

where $S_{gen,s}$ is the total entropy production rate of smooth tube.

The mathematical formulation for calculating secondary flow intensity can be expressed as [41]:

$$J_{ABS}^n = \frac{\iiint_V |\omega^n| dV}{V} \quad (25)$$

where V is the volume of the fluid domain and ω^n is component of vorticity.

2.7. Research process

Figure 2 presents the research methodology, computational workflow, and associated parametric configurations and software implementations employed in this study.

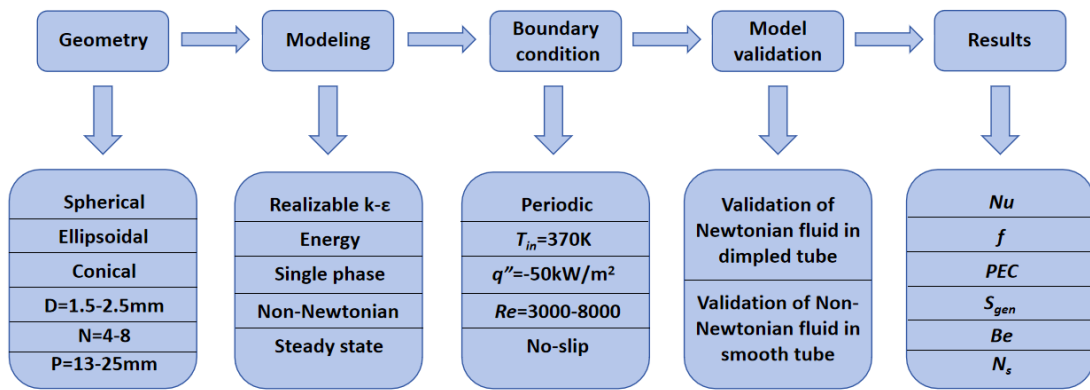


Fig. 2. Research flowchart of the study.

3. Grid independence and model validation

3.1. Grid independence

In this study, the commercial software is used to generate the hexahedral grid as shown in Fig. 3. The mesh near the wall is densified to ensure $y^+ \approx 1$. Grid independence test is conducted by using ellipsoidal dimpled enhanced tube with $N = 8$, $D = 2.5\text{mm}$, $P = 13\text{mm}$ at $Re = 8000$. The result of grid independence test is shown in Table 2. The Nu and f are almost constant when the number of grids increases from 716009 to 1078936. In order to save time while ensuring prediction accuracy, the Mesh 2 with 716009 cells is chosen.

Table 2

Grid independence test ($N = 8$, $D = 2.5\text{mm}$, $P = 13\text{mm}$, $Re = 8000$).

Mesh	Cells number	Nu	Diff, %	f	Diff, %
Mesh 1	377302	366.23	0.8	0.0990	2.8
Mesh 2	716009	368.11	0.3	0.1013	0.6
Mesh 3	1078936	369.30	Baseline	0.1019	Baseline

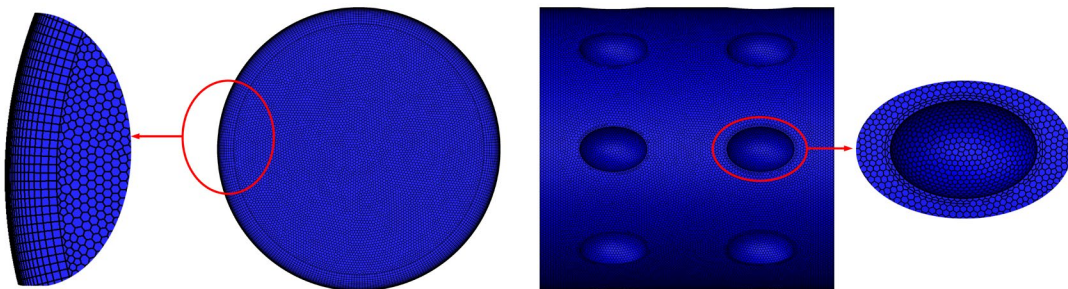


Fig. 3. Grid system of dimpled tube.

3.2. Model validation

To ensure the credibility of the simulation results, the used numerical model requires rigorous verification processes within this computational investigation. Given the absence of prior studies on thermal-hydrolyzed sewage sludge flow in dimpled tubes, this validation process comprises two stages.

First, the numerical results of Newtonian fluids in dimpled tubes are compared with the experimental results of Li et al. [42]. The results are shown in Fig. 4, where the max error for Nu and f is 8.41% and 9.83%, respectively.

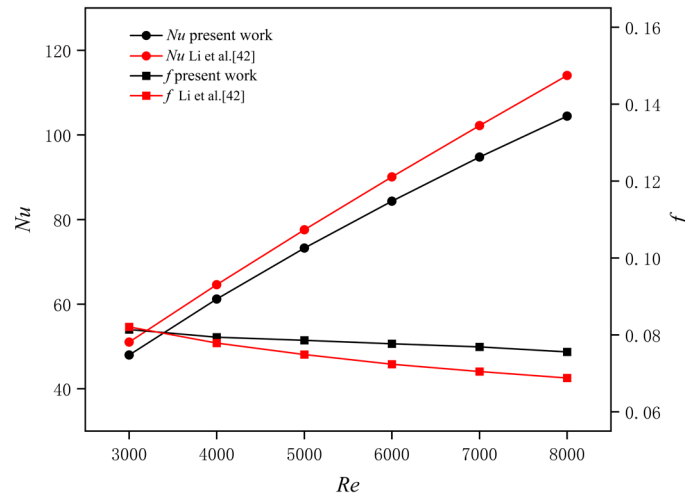


Fig. 4. Model validation of Newtonian fluid in dimpled tubes.

Second, in order to confirm that the numerical model adopted in this study is also applicable to non-Newtonian fluids in smooth tube. Nu and f were compared for the non-Newtonian fluid in smooth tube with the experimental correlations proposed by Sandall et al. [43] and Dodge et al. [44] respectively. The Eq. (26) was proposed by Sandall et al. [43] for correlating the Nusselt number of non-Newtonian power-law fluids flow in circular tubes and the Eq. (27) proposed by Dodge et al. [44], provides a correlation for the friction factor of such flows. The results are shown in Fig. 5, where the max error for Nu and f is 8.15% and 6.09%. The above verification outcomes substantiate the validity of the numerical model implemented in this investigation.

$$Nu = \frac{PrRe\sqrt{f/2}}{12.5Pr^{\frac{2}{3}} - 7.85Pr^{1/3} + 3.61\ln Pr + 5.8 + \frac{2.78}{n} \ln \left(\frac{Re\sqrt{f/2}}{90} \right)} \quad (26)$$

$$\frac{1}{\sqrt{f}} = \frac{4}{n^{0.75}} \log \left(Re f^{1-\frac{n}{2}} \right) - \frac{0.4}{n^{1.2}} \quad (27)$$

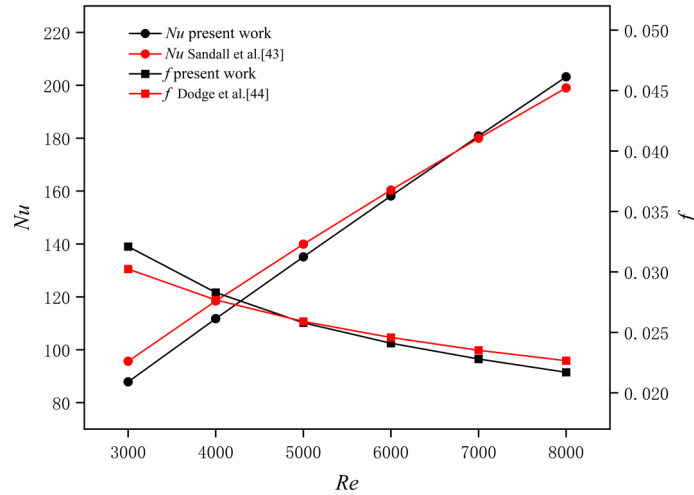


Fig. 5. Model validation of non-Newtonian fluids in smooth tubes.

4. Result and discussion

4.1. Effects of dimples shape

4.1.1. Flow and heat transfer characteristics

Figure 6 demonstrates the velocity and streamlines distributions of dimpled tubes with varying dimple shapes. From these figures, the fluid velocity within the ellipsoidal dimpled tube is the highest, followed by that in the tube with spherical and conical dimpled tubes. It is attributed to the larger volume of the ellipsoidal dimples compared to both spherical and conical dimples. Recirculation zones form on both windward and leeward surfaces of the dimple, with leeward surfaces recirculation flow rates and intensities exceeding those observed on the windward surface, this found is consistent with the Ref. [45]. Additionally, it is evident that the recirculation intensity is highest for spherical dimples, followed by ellipsoidal and conical dimples. This phenomenon is due to the greater curvature of spherical dimples compared to ellipsoidal and conical ones.

Figure 7 demonstrates the surface pressure distributions of dimpled tubes with varying dimple shapes. Under all operating conditions, the high-pressure zones consistently localize on windward surfaces of dimples, while negative pressure domains emerge at dimple vertices. Furthermore, spherical dimpled tubes, due to their greater curvature, demonstrate the highest positive and lowest negative pressures.

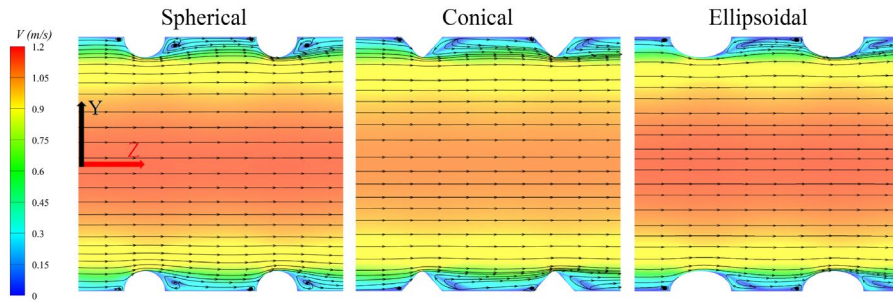


Fig. 6. Velocity and streamlines distributions of dimpled tubes with varying dimple shapes at $Re = 3000$.

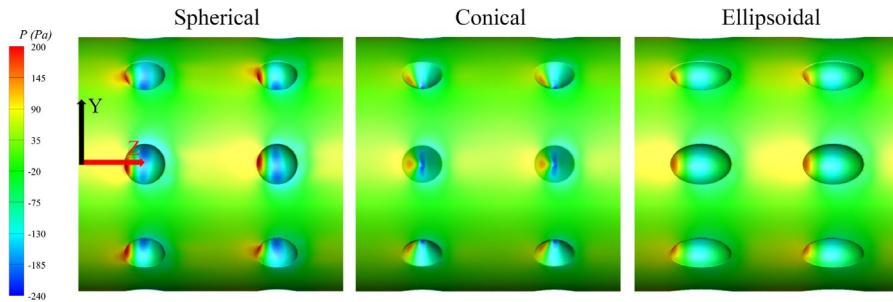


Fig. 7. Surface pressure distributions of dimpled tubes with varying dimple shapes at $Re = 3000$.

Figure 8 demonstrates the surface Nusselt number distributions for dimpled tubes with varying dimple shapes. The regions of high Nu are located upstream of the dimples. This phenomenon primarily arises from the direct impingement of upstream fluid on the dimple windward surfaces, inducing substantial boundary layer thinning [46]. The existence of flow separation leads to a notably higher surface Nu at the upstream and downstream locations of the dimples compared to the regions between adjacent radial dimples. Furthermore, comparing these figures, the surface Nu is highest at the windward side of spherical dimples, followed by ellipsoidal and conical dimples; this is also attributed to the greater curvature of spherical dimples.

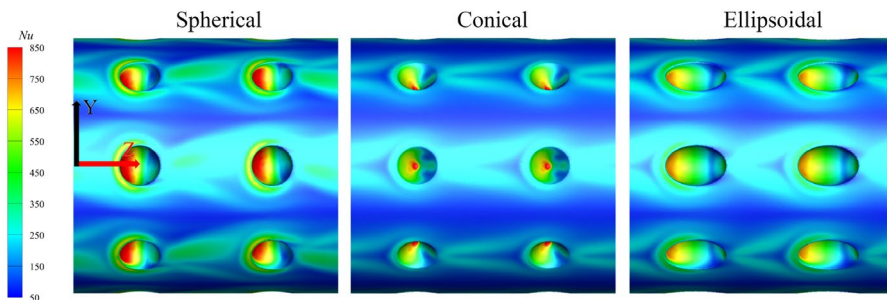
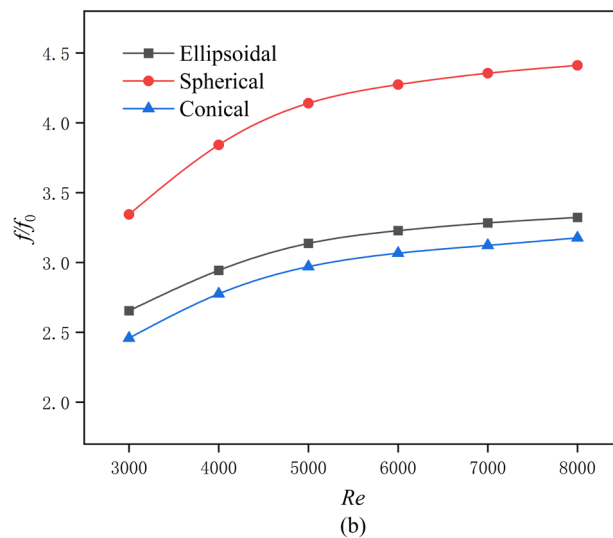
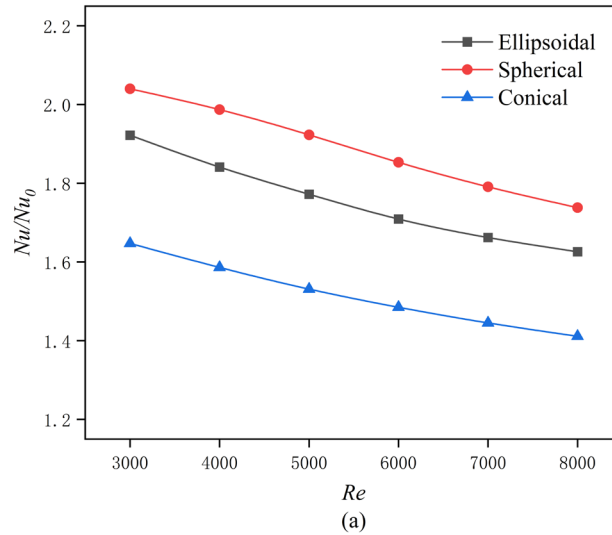


Fig. 8. Surface Nusselt number distributions of dimpled tubes with varying dimple shapes at $Re = 3000$.

4.1.2. Thermo-hydraulic performance

Figure 9 demonstrates the variation in the thermos-hydraulic performance with respect to Re for dimpled tubes with varying dimple shapes. The Nu/Nu_0 decreases as Re increases, while the f/f_0

increases for all cases. And this is consistent with the results of Li et al.[23]. Moreover, spherical dimpled tubes achieve the highest Nu/Nu_0 and ff_0 values owing to their maximum curvature. The greater the curvature, the steeper the velocity gradient becomes, thereby leading to a reduction in dynamic viscosity of fluid and an enhancement in turbulence intensity. Relative to smooth tubes, the maximum increase in Nu for spherical, ellipsoidal, and conical dimpled tubes is 2.04, 1.92, and 1.65 times, respectively, while the resistance increases by a factor of 4.41, 3.32, and 3.18 times, respectively. Within the Reynolds number range $Re = 3000\sim 8000$, ellipsoidal dimpled tubes demonstrate highest PEC values, indicating that ellipsoidal dimpled tubes exhibit better thermohydraulic performance than the others, and this is consistent with the results of Wang et al.[22]. Given that the ellipsoidal dimple configuration provides optimal thermohydraulic performance, it has been exclusively applied in all subsequent analyses presented in this study.



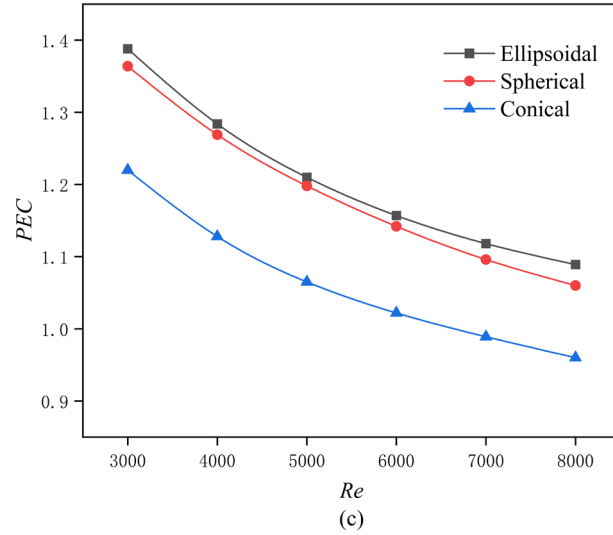


Fig. 9. Variations in thermo-hydraulic performance with respect to Re for dimpled tubes with varying dimple shapes: (a) Nu ; (b) f ; (c) PEC

4.1.3. Entropy production performance

Figure 10 demonstrates the variation entropy production performance with respect to Re for dimpled tubes with varying dimple shapes. For all cases, as Re increases, the S_{gen} and Be of the dimpled tubes decrease, while Ns increases. It is due to the increase in Re , which augments interlayer fluid mixing and attenuates axial temperature gradients within the tube, resulting in a higher heat transfer rate and a consequent decrease in thermal entropy [32]. Since $S_{gen,f}$ is relatively small compared to $S_{gen,t}$, the overall S_{gen} decreases accordingly. Furthermore, at Reynolds numbers below 7000, spherical dimpled tubes exhibit superior entropy generation characteristics compared to ellipsoidal and conical configurations. It is due to the higher heat transfer rate afforded by spherical dimples, which reduces $S_{gen,t}$. When the Re exceeds 7000, ellipsoidal dimples exhibit lower $S_{gen,f}$ than spherical dimples due to their closer conformity to streamlined shapes and consequently reduced flow resistance, the significantly higher increase rate of $S_{gen,f}$ in spherical-dimpled tubes compared to ellipsoidal configurations produces, resulting in inferior entropy generation performance of spherical dimpled tubes compared to their ellipsoidal counterparts under same working conditions.



Fig. 10. Variations in entropy production performance with respect to Re for dimpled tubes with varying dimple shapes:(a) S_{gen} ; (b) Be ; (c) N_s

4.2. Effects of dimples depth

4.2.1. Flow and heat transfer characteristics

Figure 11 demonstrates the velocity and streamlines distributions of ellipsoidal dimpled tubes

with varying dimple depths. Clearly, fluid velocity increases as dimple depths increase under same working conditions. It is because deeper dimples enlarge their volume, reducing the equivalent diameter of the dimpled tube under constant inlet conditions [45]. An increase in flow velocity can reduce the dynamic viscosity of fluid and enhance its turbulent kinetic energy. Furthermore, when comparing these figures, recirculation flow rate and intensity are increased with increasing dimple depth.

Figure 12 demonstrates the surface pressure distributions of ellipsoidal dimpled tubes with varying dimple depths. Both the positive pressure on the windward surfaces of the dimples and the negative pressure at their vertices increase in a corresponding manner as dimple depth increases. This phenomenon occurs due to increased flow blockage caused by deeper dimples.

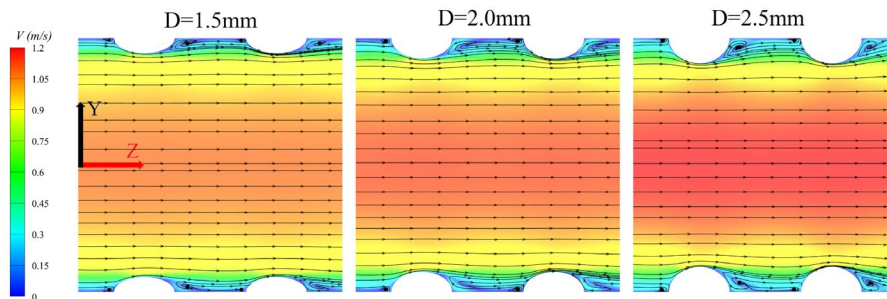


Fig. 11. Velocity and streamlines distributions of ellipsoidal dimpled tubes with varying dimple depths at $Re = 3000$.

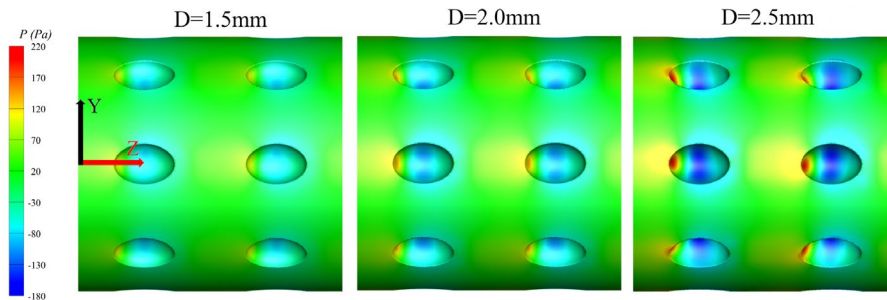


Fig. 12. Surface pressure distributions of ellipsoidal dimpled tubes with varying dimple depths at $Re = 3000$.

Figure 13 demonstrates the surface Nusselt number distributions of ellipsoidal dimpled tubes with varying dimple depths. Clearly, the surface Nu of the dimpled tubes also increase as dimple depth increases. The increase in the surface Nu at the windward surfaces of the dimples is more pronounced. It is attributed to the increase in the curvature of the windward surfaces as the dimple depth increases, resulting in more intense interactions between the fluid and the dimple surfaces.

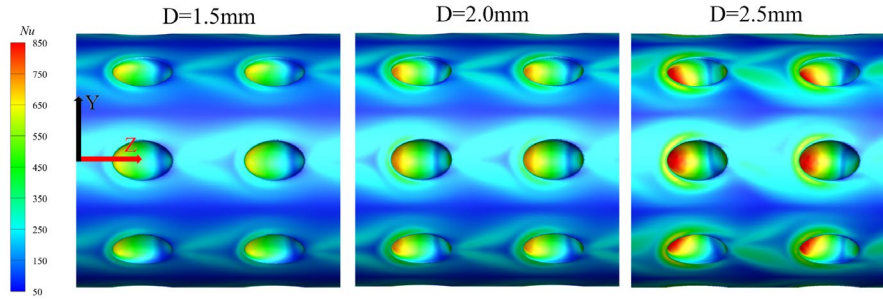
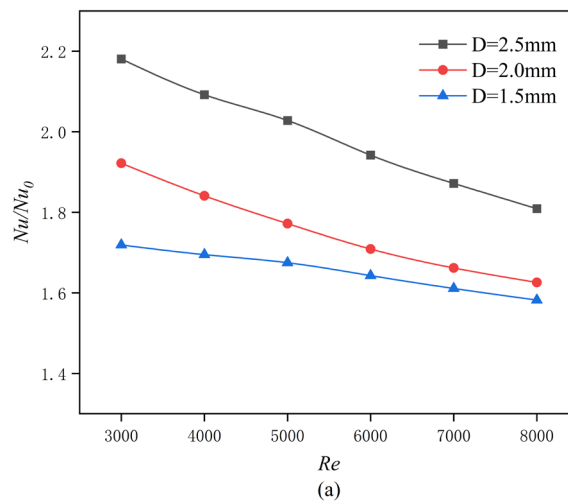


Fig. 13. Surface Nusselt number distributions of ellipsoidal dimpled tubes with varying dimple depths at $Re = 3000$.

4.2.2. Thermo-hydraulic performance

Figure 14 demonstrates the variation in thermo-hydraulic performance with respect to Re for ellipsoidal dimpled tubes with varying dimple depths. The Nu/Nu_0 decreases as Re increases, while the f/f_0 increases for all cases. Additionally, as dimple depths increase, both the heat transfer and resistance of the dimples also rise. This phenomenon occurs because the increased dimple depth causes both a reduction in the dynamic viscosity of fluid within the tube and an elevation in turbulent intensity. The dimple with the maximum depth exhibits the highest Nu/Nu_0 and f/f_0 values. Relative to smooth tubes, the maximum increase in Nu for dimpled tubes with depths $D = 1.5\text{mm}$, $D = 2.0\text{mm}$, and $D = 2.5\text{mm}$ is 1.72, 1.92, and 2.18 times, respectively, while the resistance increases by a factor of 2.57, 3.32, and 4.67 times, respectively. Within the Re range of 3000 to 8000, the ellipsoidal dimpled tube with depth $D = 1.5\text{mm}$ achieves the maximum PEC , When the Re exceeds 7000, dimpled tubes with greater dimple depths exhibit a more significant reduction in Nu/Nu_0 , while the increase in f/f_0 undergoes a relatively smaller change, resulting PEC value of dimpled tubes with depth $D = 2.0\text{mm}$ to commence exceeding that of tubes with $D = 2.5\text{mm}$.



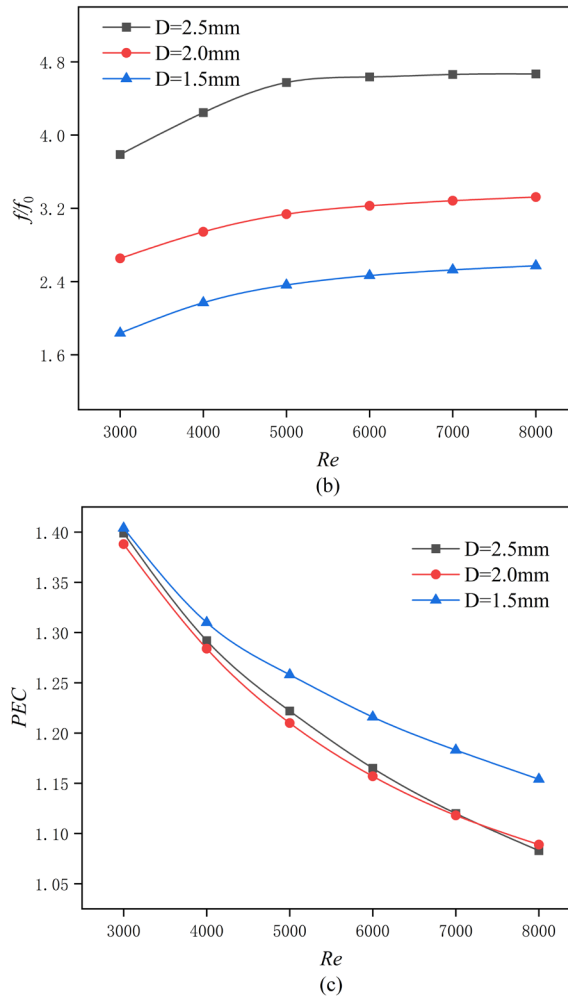


Fig. 14. Variations in thermo-hydraulic performance with Re for ellipsoidal dimpled tubes with varying dimple depths: (a) Nu ; (b) f ; (c) PEC .

4.2.3. Entropy production performance

Figure 15 demonstrates the variation in thermo-hydraulic performance with respect to Re for ellipsoidal dimpled tubes with varying dimple depths. For all cases, as Re increases, the S_{gen} and Be of the dimpled tubes decrease, while Ns increases. Overall, as dimple depths increase, the S_{gen} , Be , and Ns of the dimpled tubes all decrease. It is due to the increased heat transfer rate of the dimpled tubes, which improves temperature uniformity within the tube and reduces thermal entropy production. An increase in dimple depth enhances heat transfer of dimpled tubes within the Re range of 3000 to 6000. Conversely, exceeding $Re = 6000$ renders increased dimple depth unfavorable for heat transfer augmentation. This phenomenon occurs because deeper dimples generate greater flow resistance and consequently higher $S_{gen,f}$, with this increase being more pronounced in deeper dimples.

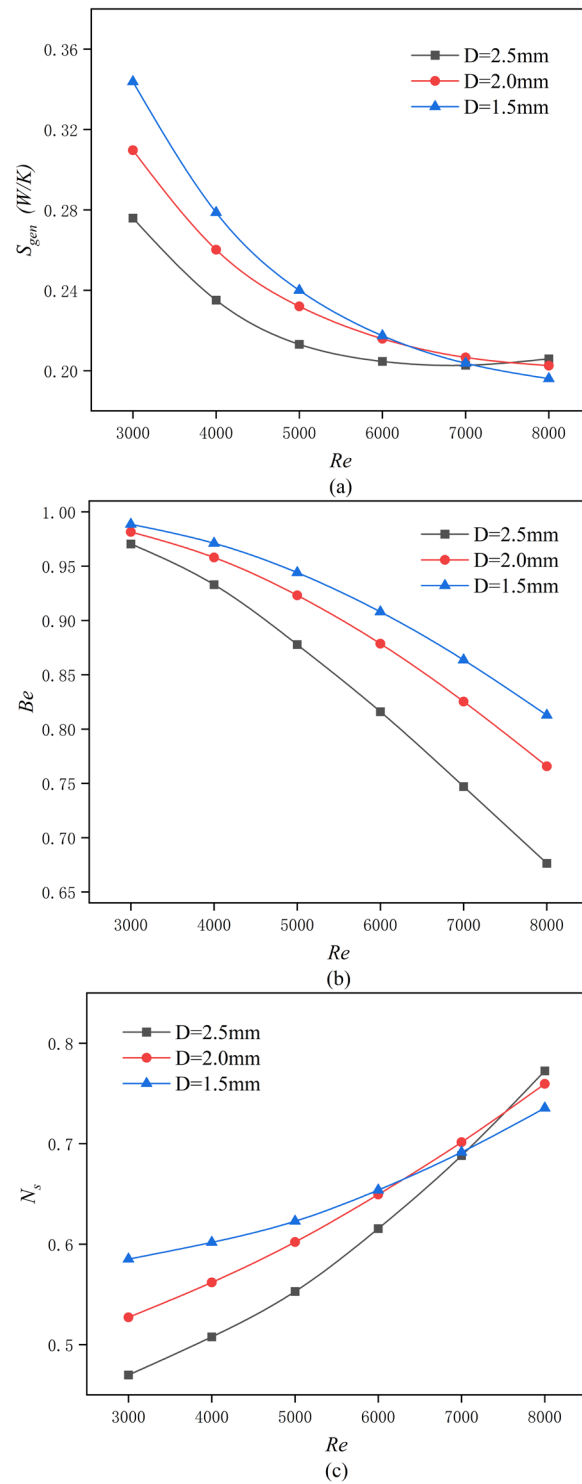


Fig. 15. Variations in entropy production performance with respect to Re for ellipsoidal dimpled tubes with varying dimple depths:(a) S_{gen} ; (b) Be ; (c) N_s .

4.3. Effects of dimples number

4.3.1. Flow and heat transfer characteristics

Figure 16 demonstrates the velocity and streamlines distributions of dimpled tubes with varying dimple numbers. The fluid velocity within the dimpled tubes increases significantly as the number

of dimples increases. It is due to the significant increase in the total volume of dimples with increasing dimple numbers. When comparing these figures, although there is no marked change in the recirculation flow per dimple, the total recirculation flow increases notably with the number of dimples, this finding aligns with that of Liao et al.[33].

Figure 17 demonstrates the surface pressure distributions of ellipsoidal dimpled tubes with varying dimple numbers. The negative pressure zones on the dimpled tube surfaces consequently multiply as the number of dimples increases. This indicates that the recirculation zones within the dimpled tubes are increased, thereby enhancing heat transfer.

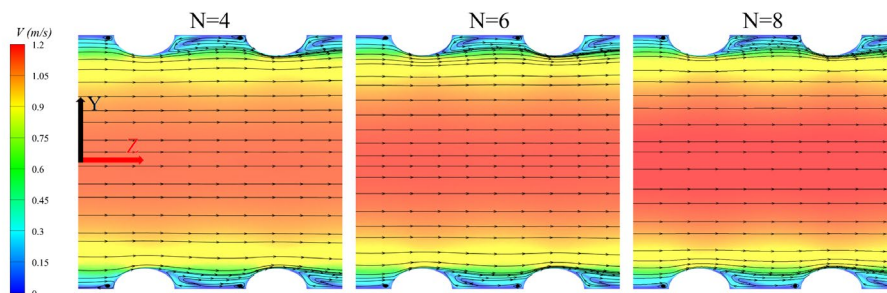


Fig. 16. Velocity and streamlines distributions of ellipsoidal dimpled tube with varying dimple numbers at $Re = 3000$.

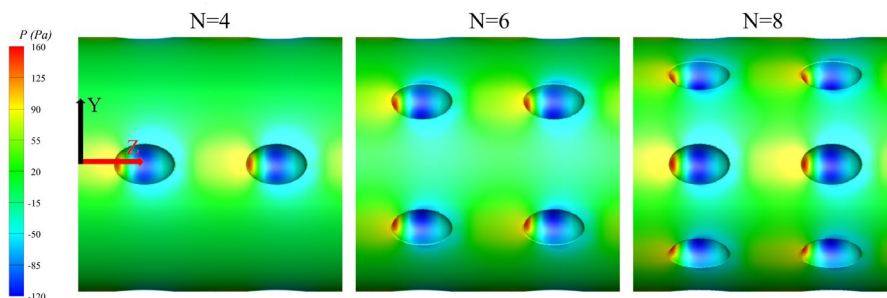


Fig. 17. Surface pressure distributions of ellipsoidal dimpled tubes with varying dimple numbers at $Re = 3000$.

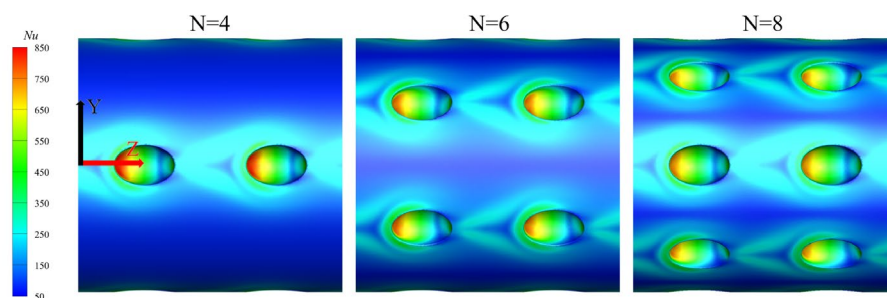


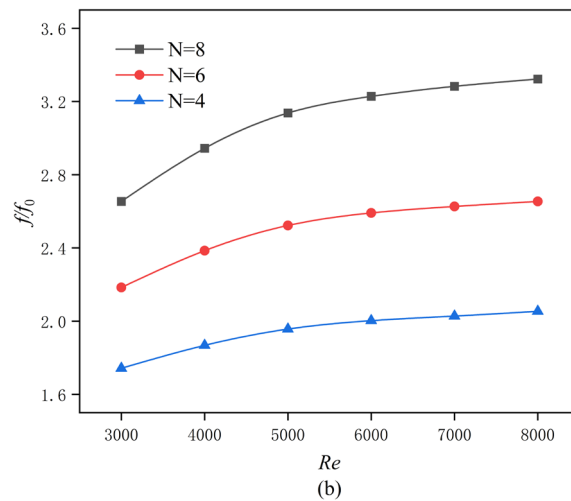
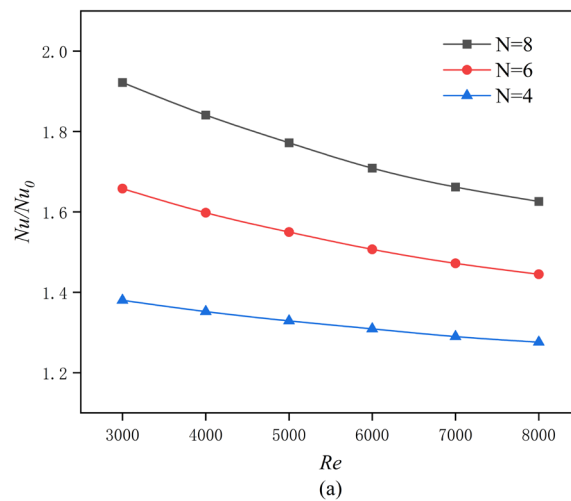
Fig. 18. Surface Nusselt number distributions of ellipsoidal dimpled tubes with varying dimple numbers at $Re = 3000$.

Figure 18 demonstrates the surface Nusselt number distributions of ellipsoidal dimpled tubes with varying dimple numbers. Clearly, the areas on the dimpled surfaces with high Nu values expand significantly as the number of dimples increases. This expansion thereby enhances the overall heat

transfer.

4.3.2. Thermo-hydraulic performance

Figure 19 demonstrates the variation in thermohydraulic performance with respect to Re for ellipsoidal dimpled tubes with varying dimple numbers. The Nu/Nu_0 decreases as Re increases, while the f/f_0 increases for all cases. Similarly, this phenomenon arises as the increased dimple count not only reduces the dynamic viscosity of fluid and elevates turbulent intensity within the tube, but also significantly expands the effective heat transfer area. Additionally, both the heat transfer and resistance of the dimples also rise as the number of dimples increases. The dimple with the maximum number exhibits the highest Nu/Nu_0 and f/f_0 values. Relative to smooth tubes, the maximum increase in Nu for dimpled tubes with dimple numbers $N = 4$, $N = 6$, and $N = 8$ is 1.38, 1.66, and 1.92 times, respectively, while the resistance increases by a factor of 2.05, 2.65, and 3.32 times, respectively. Within the Reynolds number range of 3000 to 8000, the ellipsoidal dimpled tube containing 8 transverse dimples exhibits the highest PEC value.



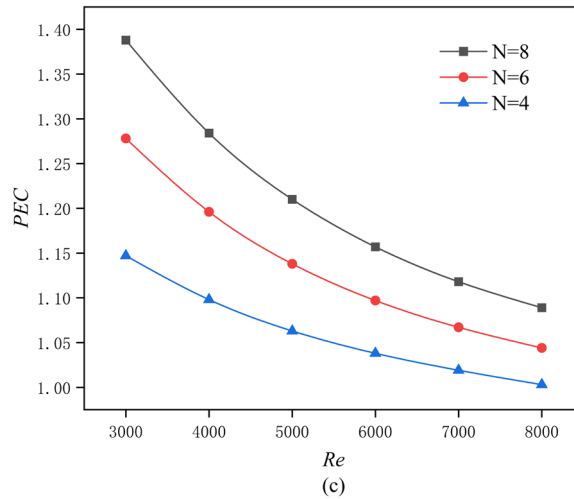
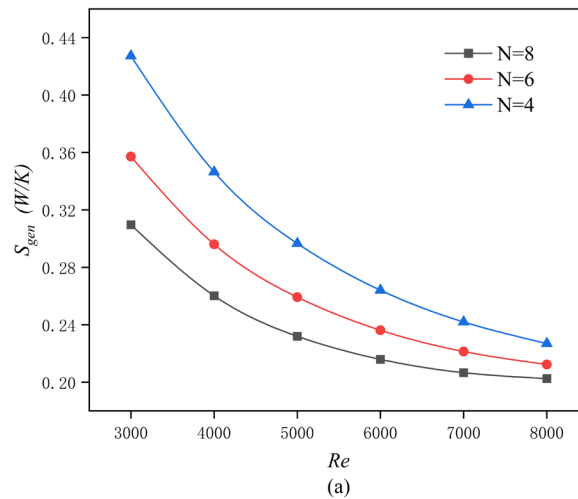


Fig. 19. Variations in thermohydraulic performance with respect to Re for ellipsoidal dimpled tubes with varying dimple numbers: (a) Nu ; (b) f ; (c) PEC .

4.3.3. Entropy production performance

Figure 20 demonstrates the variation in entropy production performance with respect to Re for ellipsoidal dimpled tubes with varying dimple numbers. For all cases, as Re increases, the S_{gen} and Be of the dimpled tubes decrease, while Ns increases. As the number of dimples increases, the S_{gen} , Be , and Ns of the dimpled tubes all decrease. It is due to the fluid within the dimpled tubes undergoing greater disturbance as the number of dimples increases, which enhances the degree of fluid mixing and improves temperature uniformity.



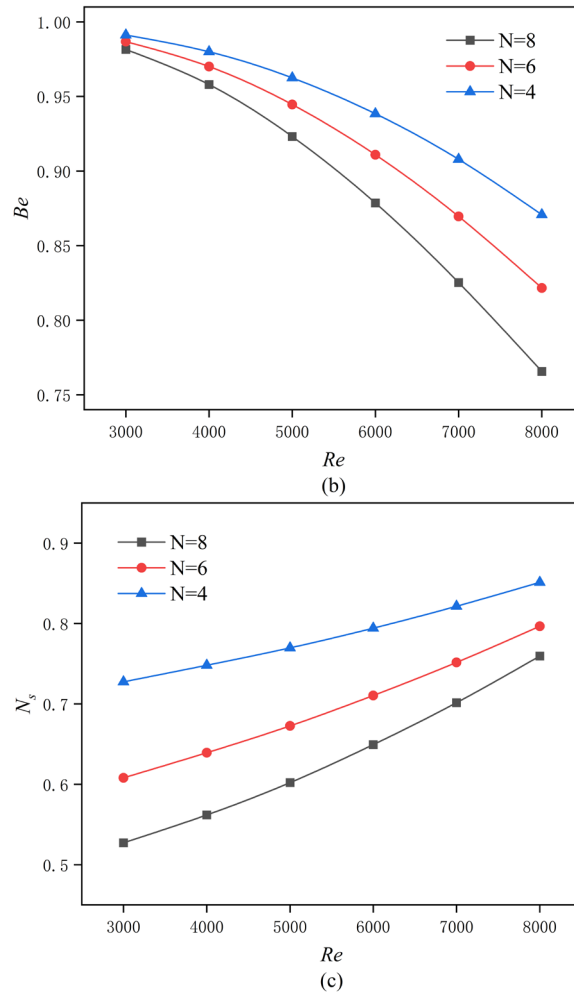


Fig. 20. Variations in entropy production performance with respect to Re for ellipsoidal dimpled tubes with varying dimple numbers:(a) S_{gen} ; (b) Be ; (c) N_s .

4.4. Effects of dimples pitch

4.4.1. Flow and heat transfer characteristics

Figure 21 demonstrates the velocity and streamlines distributions of ellipsoidal dimpled tubes with varying dimple pitches. Clearly, these figures demonstrate that as dimple pitch increases, the fluid velocity within dimpled tubes decreases significantly. This is due to the increased dimple pitch, which results in both a reduced number of dimples per unit length and a corresponding decrease in total dimple volume [45]. Furthermore, when comparing these figures, no significant variations in the recirculation flow rate and intensity are observed across varying dimple pitches.

Figure 22 demonstrates the surface pressure distributions of ellipsoidal dimpled tubes with varying dimple pitches. Clearly, these figures demonstrate that as dimple pitch increases, both the maximum positive and negative pressures rise. This behavior is attributed to the shear-thinning

nature of the fluid. The increased dimple pitch reduces the flow velocity, leading to higher fluid viscosity under shear conditions and thereby elevating the surface differential pressure.

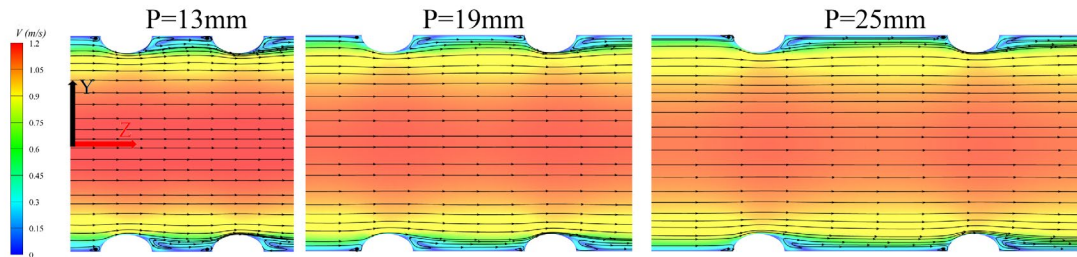


Fig. 21. Velocity and streamlines distributions of ellipsoidal dimpled tube with varying dimple pitches at $Re = 3000$.

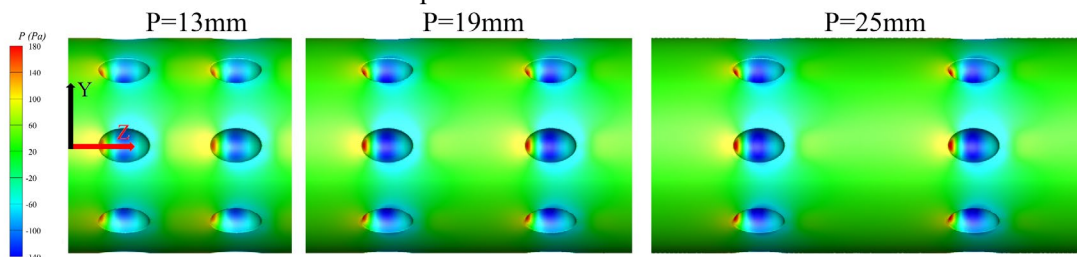


Fig. 22. Surface pressure distributions of ellipsoidal dimpled tubes with varying dimple pitches at $Re = 3000$.

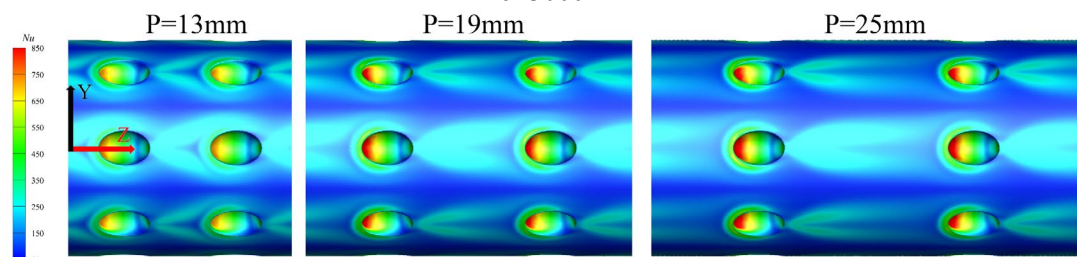


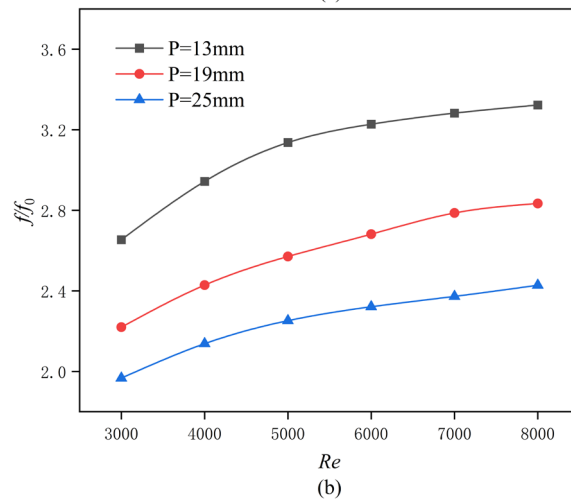
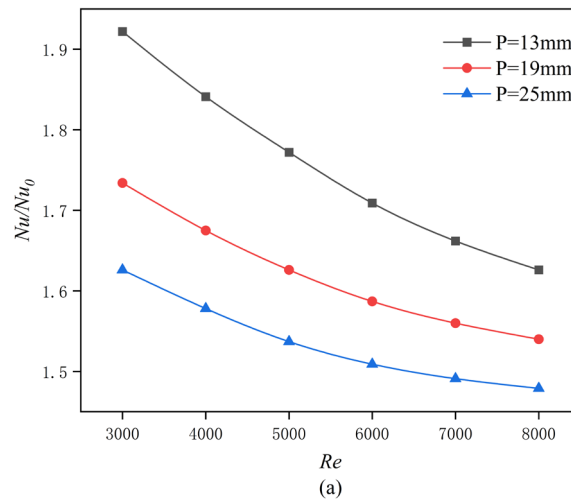
Fig. 23. Surface Nusselt number distributions of ellipsoidal dimpled tubes with varying dimple pitches at $Re = 3000$.

Figure 23 demonstrates the surface Nusselt number distributions of ellipsoidal dimpled tubes with varying dimple pitches. Clearly, these figures indicate that as dimple pitch increases, the surface Nu on the windward surfaces of the dimples also rise. It is because increasing the dimple pitch reduces interference from upstream dimples on the fluid near the front of the dimples, leading to enhanced kinetic energy levels. However, a smaller dimple pitch creates a larger area of high Nu regions, thereby improving the overall heat transfer of dimpled tubes.

4.4.2. Thermo-hydraulic performance

Figure 24 demonstrates the variation in thermo-hydraulic performance with respect to Re for ellipsoidal dimpled tubes with varying dimple pitches. The Nu/Nu_0 decreases as Re increases, while the f/f_0 increases for all cases. Additionally, as the dimple pitch increases, both the heat transfer and resistance of the dimples also decrease. Similarly, this phenomenon occurs because the increase in

dimple spacing causes an increase in the dynamic viscosity of fluid and a decrease in turbulent intensity within the tube, while also resulting in a reduction in the heat transfer area per unit length. The dimple with the minimum pitch exhibits the highest Nu/Nu_0 and f/f_0 values. Relative to smooth tubes, the maximum increase in Nu for dimpled tubes with dimple pitches $P = 13\text{mm}$, $P = 19\text{mm}$, and $P = 25\text{mm}$ is 1.92, 1.73, and 1.63 times, respectively, while the resistance increases by a factor of 3.32, 2.83, and 2.43 times, respectively. Within the Re range of 3000 to 7000, the ellipsoidal dimpled tube with $P = 13\text{mm}$ achieves the maximum PEC . When the Re exceeds 7000, dimpled tubes with greater dimple pitches exhibit a more significant reduction in Nu/Nu_0 , while the increase in f/f_0 undergoes a relatively smaller change, resulting the ellipsoidal dimpled tube with $P = 25\text{mm}$ exhibits the highest PEC value.



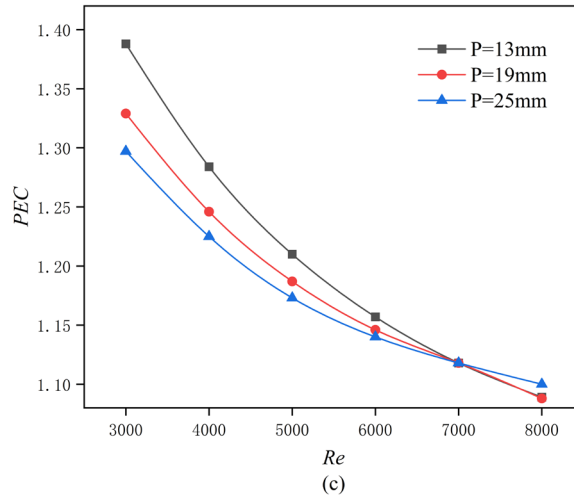
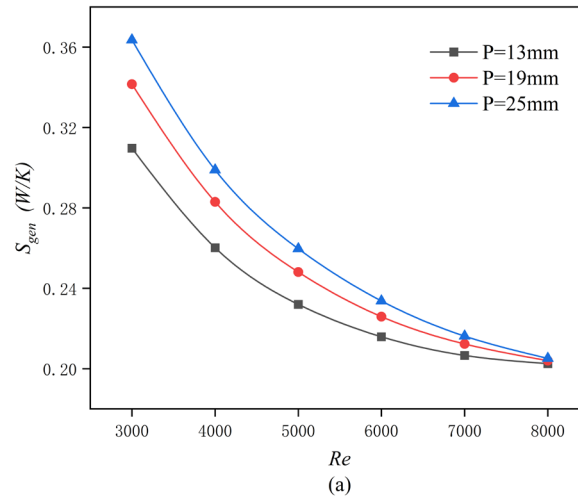


Fig. 24. Variations in thermos-hydraulic performance with respect to Re for ellipsoidal dimpled tubes with varying dimple pitches: (a) Nu ; (b) f ; (c) PEC .

4.4.3. Entropy production performance

Figure 25 demonstrates the variation in entropy production performance with respect to Re for ellipsoidal dimpled tubes with varying dimple pitches. For all cases, as Re increases, the S_{gen} and Be of the dimpled tubes decrease, while Ns increases. As dimple pitch increases, the S_{gen} , Be , and Ns of the dimpled tubes all increase. It is due to the diminished fluid mixing and temperature uniformity caused by the increased dimple pitch, which worsens the overall temperature distribution within the system.



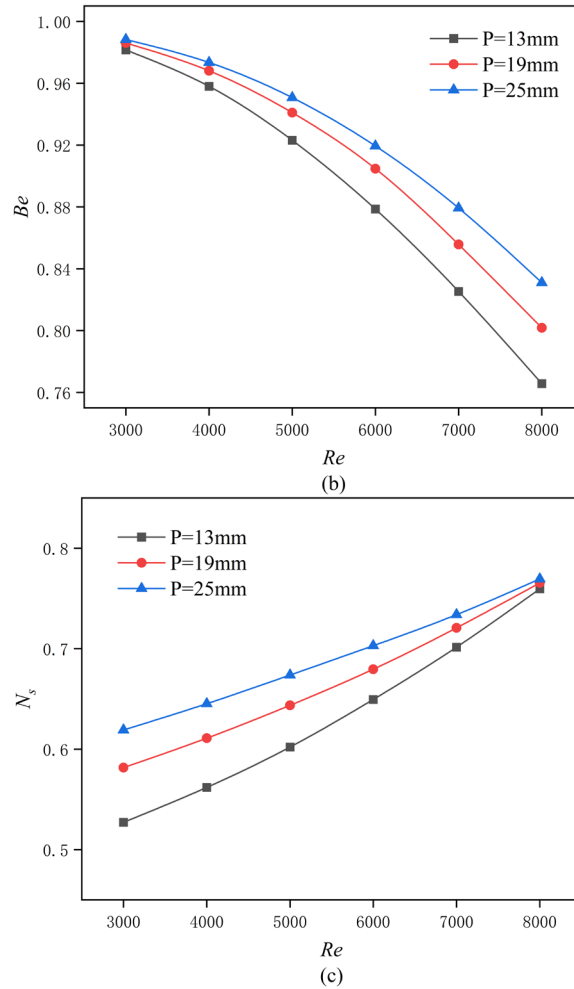


Fig. 25. Variations in entropy production performance with respect to Re for ellipsoidal dimpled tubes with varying pitches:(a) S_{gen} ; (b) Be ; (c) N_s .

4.5. Enhanced heat transfer mechanism

For non-Newtonian fluids, viscosity varies with flow conditions. Lower fluid viscosity reduces the boundary layer thickness, thereby enhancing heat transfer efficiency. Fig. 26 demonstrates the dynamic viscosity distribution of smooth tube and ellipsoidal dimpled tube. Dimpled tube exhibits lower fluid dynamic viscosity compared to smooth tube, with this viscosity diminution consistently observed throughout the entire cross-sectional domain, encompassing both near-wall regions and central flow zones. Furthermore, higher velocity gradients in the windward and leeward regions of the dimples lead to lower dynamic viscosity compared to other areas. This suggests that the presence of these high velocity gradient regions reduces the boundary layer thickness, thereby improving heat transfer efficiency.

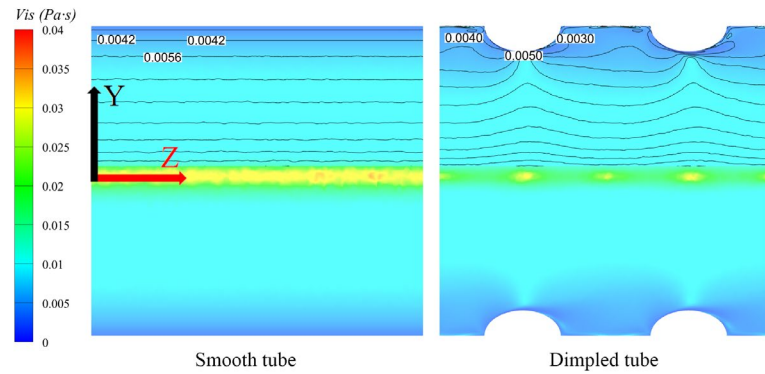


Fig. 26. Dynamic viscosity distribution of smooth tube and ellipsoidal dimpled tube with $D = 2.0$ mm, $N = 8$, $P = 13$ mm at $Re = 3000$.

A quantitative analysis was conducted to examine the average dynamic viscosity variations of the fluid within smooth tubes and dimpled tubes, as illustrated in Fig. 27. As shown, all dimpled tubes exhibit lower dynamic viscosity values relative to smooth tubes, with a progressive decrease as Re increases. This is due to the inherent shear-thinning rheological behavior of thermally hydrolyzed sewage sludge, where apparent viscosity decreases monotonically with increasing shear rate. Under invariant geometric constraints ($D = 2.0$ mm, $N = 8$, $P = 13$ mm), ellipsoidal dimpled tubes demonstrated lower average dynamic viscosity. This indicates that the ellipsoidal dimple configuration induces significantly higher shear rates within the tube compared to other profiles. Within the investigated parameter ranges, averaged data reveal that: A 33% increase in dimple depth reduces average dynamic viscosity by 4.7%; A 50% increase in dimple number reduces average dynamic viscosity by 2.6%; A 46% expansion in dimple pitch elevates average dynamic viscosity by 2.1%. Therefore, the relative influence of dimple geometric parameters on average dynamic viscosity follows a hierarchy: $D > N > P$.

The primary distinction between non-Newtonian and Newtonian fluids lies in the variation of viscosity with shear rate for non-Newtonian fluids. For shear-thinning fluids, viscosity reaches its minimum near the tube wall due to the velocity distribution, a phenomenon also demonstrated in Figure 26. Dimples enhance the fluid velocity gradient, reduce fluid viscosity, thin the boundary layer, and consequently improve heat transfer efficiency. Compared to Newtonian fluids with identical consistency coefficients (in the power-law model, the dynamic viscosity of Newtonian fluids equals the consistency coefficient K , with the power-law index $n = 1$.), dimples further amplify the heat transfer coefficient in non-Newtonian fluids. Concurrently, the inherent properties of shear-thinning fluids result in a lower pressure drop than Newtonian fluids with equivalent

consistency coefficients.

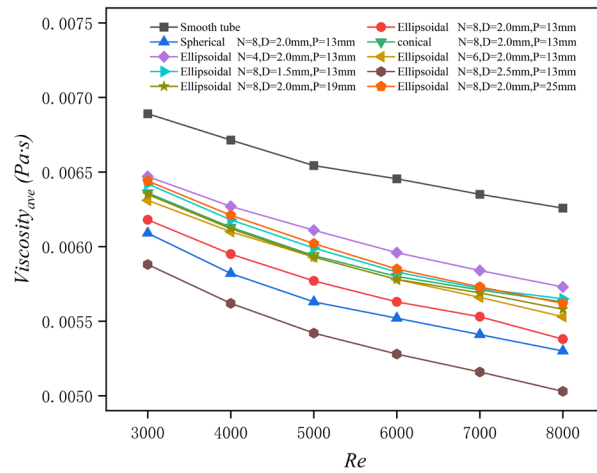


Fig. 27 Variation of average dynamic viscosity with Re for all dimpled tubes.

The thermal performance enhancement mechanism in dimpled tubes originates from surface dimples inducing flow separation and vortex generation, enhancing fluid mixing while disrupting thermal boundary layer development. Besides, the presence of dimples increases the heat transfer area, achieving higher heat transfer [47-49]. The vortical flow induced by dimples is categorized as a form of secondary flow. Consequently, a quantitative analysis of secondary flow intensity within the dimpled tubes were conducted, with the computational results systematically presented in Fig. 28.

Figure 28 illustrates that secondary flow intensity intensifies with increasing Re . Under invariant geometric constraints ($D = 2.0$ mm, $N = 8$, $P = 13$ mm), ellipsoidal dimpled tubes demonstrate higher absolute average vorticity. Within the investigated parameter ranges, the averaged data reveal that: A 33% increase in dimple depth enhances secondary flow intensity by 9%; A 50% augmentation in dimple number elevates secondary flow intensity by 5.5%; A 46% expansion in dimple pitch reduces secondary flow intensity by 4.4%. Therefore, the relative influence of dimple geometric parameters on secondary flow intensity follows a hierarchy: $D > N > P$.

Figure 29 demonstrates the secondary flow distribution of smooth tube and ellipsoidal dimpled tube. As observed in the figure, no secondary flow exists in the smooth tube, whereas distinct secondary flows are evident near the dimpled surfaces of the dimples. The intensity of these secondary flows gradually declines as the distance from the dimples increases. These flow structures enhance fluid mixing through rotational momentum transfer, thereby improving heat transfer

efficiency via intensified fluid mixing and thermal convection processes.

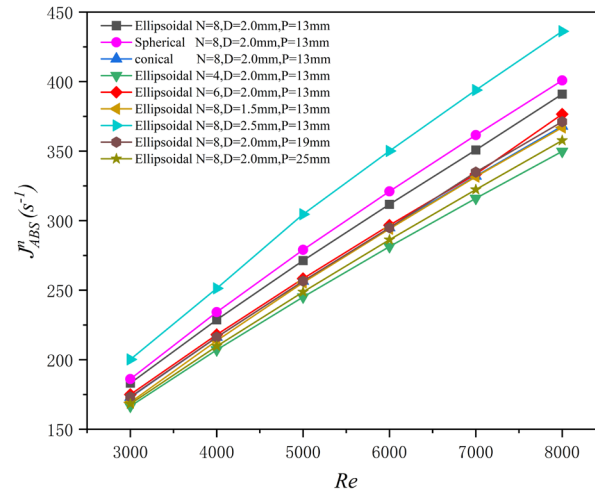


Fig. 28 Variation in secondary flow intensity with Re for all dimpled tubes.

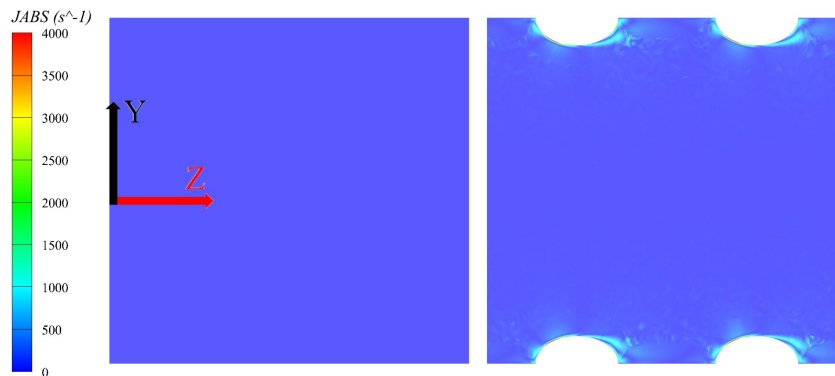


Fig. 29. Secondary flow distribution of smooth tube and ellipsoidal dimpled tube with $D = 2.0$ mm, $N = 8$, $P = 13$ mm at $Re = 3000$.

Turbulent kinetic energy serves as an indicator of flow turbulence intensity within tube. Enhanced turbulent kinetic energy levels promote more fluid momentum exchange, consequently elevating both f and Nu . Figure 30 demonstrates the turbulent kinetic energy distribution for smooth tube and ellipsoidal dimpled tube. As shown, the turbulent kinetic energy in the smooth tube is lower and more uniformly distributed, whereas in the dimpled tube, the fluid exhibits regions of higher turbulent kinetic energy in the leeward zones of the dimples. These high-energy regions extend into the downstream windward areas of the dimples. This observation indicates that energy exchange near the dimples exhibits significant intensity, thereby enhancing heat transfer efficiency.

Figure 31 quantifies the averaged turbulent kinetic energy of fluid flow in dimpled tubes under varying geometric parameters. The analysis shows that dimpled configurations universally exhibit higher averaged turbulent kinetic energy than smooth tubes and increases with increasing Re . Furthermore, the average turbulent kinetic energy exhibits enhancement with increasing dimple

depth and number, while showing a negative correlation with decreasing dimple pitch. Under invariant geometric constraints ($D = 2.0$ mm, $N = 8$, $P = 13$ mm), ellipsoidal dimpled tubes demonstrated higher turbulent kinetic energy. Within the investigated parameter ranges, the averaged data reveal that: A 33% increase in dimple depth amplifies the average turbulent kinetic energy by 36%; A 50% increase in dimple number enhances turbulence intensity by 27%; A 46% increase in dimple pitch reduces the average turbulent kinetic energy by 15%. Therefore, the relative influence of dimple geometric parameters on the average turbulent kinetic energy follows a hierarchy: $D > N > P$.

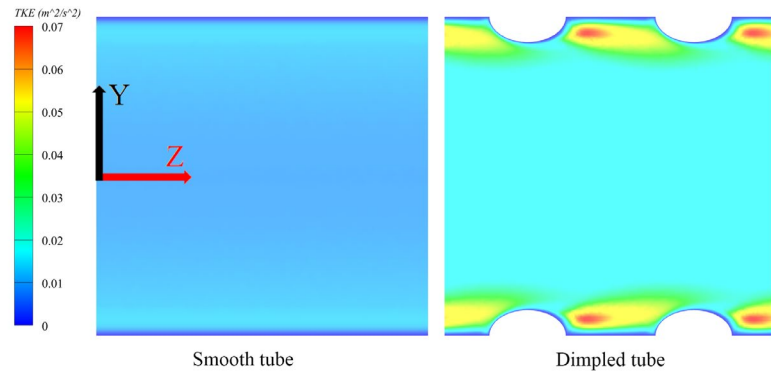


Fig. 30. *TKE* distribution for smooth tube and ellipsoidal dimpled tube with $D = 2.0$ mm, $N = 8$, $P = 13$ mm at $Re = 3000$.

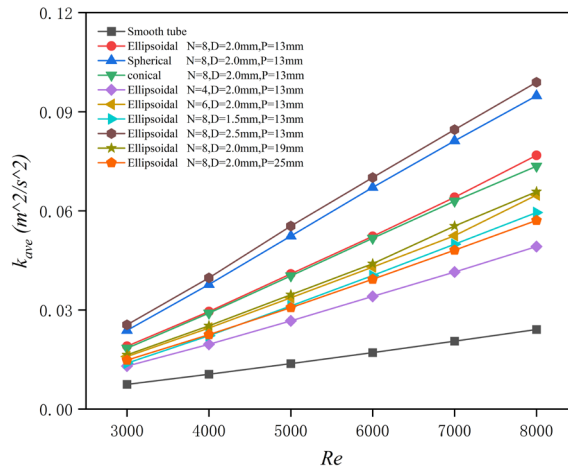


Fig. 31 Variation of average turbulent kinetic energy with Re for all dimpled tubes.

5. Conclusions

This study investigates the performance and entropy generation characteristics of waste heat recovery from thermally hydrolyzed sewage sludge with non-Newtonian fluid properties using dimpled tubes with varied geometric parameters (shape, depth, number, and pitch) through numerical simulations. A quantitative assessment was conducted to investigate the effects of these

structural parameters on the turbulent kinetic energy, secondary flow intensity, and dynamic viscosity characteristics within sewage sludge systems. The following conclusions were derived:

- (1) From a thermal-hydraulic performance perspective, the ellipsoidal dimpled tube demonstrates superior performance. In general, an increase in number, and a reduction in dimple depth and dimple pitch, is observed to contribute to enhanced *PEC* values. The ellipsoidal dimpled tube with $D = 1.5\text{mm}$, $N = 8$, $P = 13\text{mm}$ has the maximum *PEC* value of 1.404 at $Re=3000$.
- (2) From an entropy production performance perspective, spherical dimpled tubes exhibit the most favorable thermodynamic characteristics, the N_s value reaches a minimum of 0.499. In general, an increase in dimple depth and number, and a reduction in dimple pitch, is observed to contribute to enhanced entropy production performance. The ellipsoidal dimpled tube with $D = 2.5\text{mm}$, $N = 8$, $P = 13\text{mm}$ has the maximum N_s value of 0.469 at $Re=3000$.
- (3) Among the structural parameters of dimple depth, dimple number, and dimple pitch, dimple depth has the greatest influence on the performance of dimpled tubes, while dimple pitch has the least impact, the relative influence of dimple geometric parameters on various performances exhibits a hierarchy of $D > N > P$.

Acknowledgements

This work was supported by the National Natural Science Foundation of China (52370149), National Engineering Research Centre of New Energy Vehicles, and Power Systems and Shanghai Key Lab of Vehicle Aerodynamics and Vehicle Thermal Management Systems, and Science and technology innovation project of Hunan Province (2022RC4020), Natural Science Foundation of Shanghai (22ZR1442700).

References

- [1] G. Zhen, X. Lu, H. Kato, Y. Zhao, Y.-Y. Li, Overview of pretreatment strategies for enhancing sewage sludge disintegration and subsequent anaerobic digestion: Current advances, full-scale application and future perspectives, *Renewable and Sustainable Energy Reviews* 69 (2017) 559–577.
- [2] G. Zhang, Y. Shi, W. Chen, M. Dou, Z. Zhao, X. Wang, T. Zhang, Methane production from waste activated sludge by combining calcium peroxide pretreatment with zero valent iron bio-enhancement: Performance and mechanisms, *Journal of Cleaner Production* 320 (2021) 128773.
- [3] O. Eljamal, R. Eljamal, O. Falyouna, I. Maamoun, I.P. Thompson, Exceptional contribution of iron nanoparticle and aloe vera biomass additives to biogas production from anaerobic digestion of waste sludge, *Energy* 302 (2024) 131761.
- [4] Y. Zhang, S. Hu, J. Li, M. Liu, L. Xu, L. Li, Q. He, L. Gu, Sodium disilicate pretreatment enhancing methane production from anaerobic digestion of waste activated sludge, *Chemical Engineering Journal* 497 (2024) 154354.

- [5] H. Carrère, C. Dumas, A. Battimelli, D.J. Batstone, J.P. Delgenès, J.P. Steyer, I. Ferrer, Pretreatment methods to improve sludge anaerobic degradability: A review, *Journal of Hazardous Materials* 183 (2010) 1–15.
- [6] G. Kor-Bicakci, C. Eskicioglu, Recent developments on thermal municipal sludge pretreatment technologies for enhanced anaerobic digestion, *Renewable and Sustainable Energy Reviews* 110 (2019) 423–443.
- [7] S.M. Mirsoleimani Azizi, N. Haffiez, A. Mostafa, A. Hussain, M. Abdallah, A. Al-Mamun, A. Bhatnagar, B.R. Dhar, Low- and high-temperature thermal hydrolysis pretreatment for anaerobic digestion of sludge: Process evaluation and fate of emerging pollutants, *Renewable and Sustainable Energy Reviews* 200 (2024) 114453.
- [8] R. Cano, A. Nielfa, M. Fdz-Polanco, Thermal hydrolysis integration in the anaerobic digestion process of different solid wastes: Energy and economic feasibility study, *Bioresource Technology* 168 (2014) 14–22.
- [9] W.P.F. Barber, Thermal hydrolysis for sewage treatment: A critical review, *Water Research* 104 (2016) 53–71.
- [10] S.M. Mirsoleimani Azizi, B.S. Zakaria, B.R. Dhar, Low-temperature thermal hydrolysis for enhancing sludge anaerobic digestion and antibiotic resistance management: Significance of digester solids retention time, *Science of The Total Environment* 917 (2024) 170392.
- [11] T. Hidaka, M. Nakamura, F. Oritate, F. Nishimura, Comparative anaerobic digestion of sewage sludge at different temperatures with and without heat pre-treatment, *Chemosphere* 307 (2022) 135808.
- [12] P. GaneshKumar, S. VinothKumar, V.S. Vigneswaran, S.C. Kim, V. Ramkumar, Advancing heat exchangers for energy storage: A comprehensive review of methods and techniques, *Journal of Energy Storage* 99 (2024) 113334.
- [13] K. Song, Q. Yang, K. Sun, X. Wu, Q. Zhang, Q. Hou, Performance promotion by novel fin configurations with ellipsoidal dimple-protrusion for a circle tube-fin heat exchanger, *International Communications in Heat and Mass Transfer* 157 (2024) 107731.
- [14] S. Pourahmad, S.M. Pesteei, Effectiveness-NTU analyses in a double tube heat exchanger equipped with wavy strip considering various angles, *Energy Convers. Manage.* 123 (2016) 462–469.
- [15] M. Babaelahi, S. Sadri, O. Al-Jaberi, Numerical modeling and multi-objective optimization of helically grooved tube geometry in shell-and-tube heat exchangers: A comprehensive analysis of heat transfer enhancement, turbulence characteristics, and pressure drop using COMSOL multiphysics, *Chemical Engineering Science* 311 (2025) 121638.
- [16] Z.S. Kareem, S. Abdullah, T.M. Lazim, M.N. Mohd Jaafar, A.F. Abdul Wahid, Heat transfer enhancement in three-start spirally corrugated tube: Experimental and numerical study, *Chemical Engineering Science* 134 (2015) 746–757.
- [17] D. Zhang, H. Tao, C. Yao, Z. Sun, Effects of residence time on the efficiency of desulfurization and denitrification in the bubbling reactor, *Chemical Engineering Science* 174 (2017) 203–221.
- [18] P. Promvong, Thermal augmentation in circular tube with twisted tape and wire coil turbulators, *Energy Conversion and Management* 49 (2008) 2949–2955.
- [19] A. Khashaei, M. Ameri, S. Azizifar, M.H. Cheraghi, Experimental investigation on the heat transfer augmentation and friction factor inside tube enhanced with deep dimples, *International Communications in Heat and Mass Transfer* 149 (2023) 107149.
- [20] Y. Eng, C.M.J. Tay, B.C. Khoo, Drag and heat transfer in turbulent channel flow over shallow circular dimples: The shift of the deepest point of dimples, *International Journal of Thermal Sciences* 185 (2023) 108049.
- [21] S.A. Abtahi Mehrjardi, K. Mazaheri, Numerical investigation on dimpled tube effects on internal cooling performance of turbine blades, *Applied Thermal Engineering* 252 (2024) 123635.
- [22] Y. Wang, Y.-L. He, Y.-G. Lei, J. Zhang, Heat transfer and hydrodynamics analysis of a novel dimpled tube, *Experimental Thermal and Fluid Science* 34 (2010) 1273–1281.
- [23] M. Li, T.S. Khan, E. Al Hajri, Z.H. Ayub, Geometric optimization for thermal-hydraulic performance of dimpled enhanced tubes for single phase flow, *Applied Thermal Engineering* 103 (2016) 639–650.
- [24] R. Sabir, M.M. Khan, M. Imran, N.A. Sheikh, M. Irfan, Role of transverse dimples in thermal-hydraulic performance of dimpled enhanced tubes, *International Communications in Heat and*

- Mass Transfer 139 (2022) 106435.
- [25] L. Zhang, W. Xiong, J. Zheng, Z. Liang, S. Xie, Numerical analysis of heat transfer enhancement and flow characteristics inside cross-combined ellipsoidal dimple tubes, *Case Studies in Thermal Engineering* 25 (2021) 100937.
- [26] P.G. Vicente, A. García, A. Viedma, Heat transfer and pressure drop for low Reynolds turbulent flow in helically dimpled tubes, *International Journal of Heat and Mass Transfer* 45 (2002) 543–553.
- [27] K. Aroonrat, S. Wongwises, Experimental investigation of condensation heat transfer and pressure drop of R-134a flowing inside dimpled tubes with different dimpled depths, *International Journal of Heat and Mass Transfer* 128 (2019) 783–793.
- [28] E. Gürsoy, M. Tan, M. Gürdal, Y. Çetinceviz, Python-based machine learning estimation of thermo-hydraulic performance along varying nanoparticle shape, nanofluid and tube configuration, *Advances in Engineering Software* 199 (2025) 103814.
- [29] E. Gürsoy, H.K. Pazarlıoğlu, M. Gürdal, E. Gedik, K. Arslan, Parametric analysis of different Al₂O₃ nanoparticle shapes and expansion angles for sudden expanded tube regarding the first law of thermodynamics, *International Journal of Thermal Sciences* 197 (2024) 108759.
- [30] E. Gürsoy, H.K. Pazarlıoğlu, M. Gürdal, E. Gedik, K. Arslan, Entropy generation of ferro-nanofluid flow in industrially designed bended dimpled tube, *Thermal Science and Engineering Progress* 37 (2023) 101620.
- [31] H.K. Pazarlıoğlu, E. Gürsoy, M. Gürdal, M. Tekir, E. Gedik, K. Arslan, E. Taşkesen, The first and second law analyses of thermodynamics for CoFe₂O₄/H₂O flow in a sudden expansion tube inserted elliptical dimpled fins, *International Journal of Mechanical Sciences* 246 (2023) 108144.
- [32] A. Kaood, A. ElDegwy, A. Aboulmagd, Hydrothermal and entropy generation performance of convergent tubes with various dimple shapes, *International Journal of Thermal Sciences* 197 (2024) 108842.
- [33] W. Liao, X. Liu, G. Li, T. Chen, Evaluation of thermal-hydraulic performance of dimpled tube from the perspective of skewness and kurtosis, *International Journal of Thermal Sciences* 156 (2020) 106469.
- [34] W. Lin, Z. Ling, X. Fang, X. Gao, Z. Zhang, Numerical investigation on non-newtonian fluid flowing in heat exchanger with different elliptic aspect ratios and helical angles, *Appl. Therm. Eng.* 141 (2018) 164–173.
- [35] V. Lotito, L. Spinosa, G. Mininni, R. Antonacci, The rheology of sewage sludge at different steps of treatment, *Water Science and Technology* 36 (1997) 79–85.
- [36] J. Chen, Z. Hai, X. Lu, C. Wang, X. Ji, Heat-transfer enhancement for corn straw slurry from biogas plants by twisted hexagonal tubes, *Applied Energy* 262 (2020) 114554.
- [37] S. Xie, Z. Liang, L. Zhang, Y. Wang, A numerical study on heat transfer enhancement and flow structure in enhanced tube with cross ellipsoidal dimples, *International Journal of Heat and Mass Transfer* 125 (2018) 434–444.
- [38] M. Hojjat, S.G. Etemad, R. Bagheri, J. Thibault, Turbulent forced convection heat transfer of non-newtonian nanofluids, *Experimental Thermal and Fluid Science* 35 (2011) 1351–1356.
- [39] H.K. Pazarlıoğlu, E. Gürsoy, M. Gürdal, M. Tekir, E. Gedik, K. Arslan, E. Taşkesen, The first and second law analyses of thermodynamics for CoFe₂O₄/H₂O flow in a sudden expansion tube inserted elliptical dimpled fins, *International Journal of Mechanical Sciences* 246 (2023) 108144.
- [40] K. Kumar, R. Kumar, R.S. Bharj, Z. Said, Effect of arc corrugation initiation on the thermo-hydraulic performance and entropy generation of the corrugated tube, *International Communications in Heat and Mass Transfer* 138 (2022) 106335.
- [41] K.W. Song, L.B. Wang, The Effectiveness of Secondary Flow Produced by Vortex Generators Mounted on Both Surfaces of the Fin to Enhance Heat Transfer in a Flat Tube Bank Fin Heat Exchanger, *Journal of Heat Transfer* 135(4) (2013) 041902.
- [42] M. Li, T.S. Khan, E. Al-Hajri, Z.H. Ayub, Single phase heat transfer and pressure drop analysis of a dimpled enhanced tube, *Applied Thermal Engineering* 101 (2016) 38–46.
- [43] O.C. Sandall, O.T. Hanna, K. Amarnath, Experiments on turbulent non-newtonian mass transfer in a circular tube, *AIChE Journal* 32 (1986) 2095–2098.
- [44] D.W. Dodge, A.B. Metzner, Turbulent flow of non-newtonian systems, *AIChE Journal* 5 (1959) 189–204.

- [45] Z. Liang, S. Xie, L. Zhang, J. Zhang, Y. Wang, Y. Yin, Influence of geometric parameters on the thermal hydraulic performance of an ellipsoidal protruded enhanced tube, *Numerical Heat Transfer, Part A: Applications* 72 (2017) 153 - 170.
- [46] S. Xie, Z. Liang, J. Zhang, L. Zhang, Y. Wang, H. Ding, Numerical investigation on flow and heat transfer in dimpled tube with teardrop dimples, *International Journal of Heat and Mass Transfer* 131 (2019) 713 - 723.
- [47] S.A. Isaev, A.V. Schelchikov, A.I. Leontiev, Y.F. Gortyshov, P.A. Baranov, I.A. Popov, Vortex heat transfer enhancement in the narrow plane-parallel channel with the oval-trench dimple of fixed depth and spot area, *International Journal of Heat and Mass Transfer* 109 (2017) 40–62.
- [48] M. Shafae, H. Mashouf, A. Sarmadian, S.G. Mohseni, Evaporation heat transfer and pressure drop characteristics of R-600a in horizontal smooth and helically dimpled tubes, *Applied Thermal Engineering* 107 (2016) 28–36.
- [49] M. Gürdal, H.K. Pazarlıoğlu, M. Tekir, F.M. Altunay, K. Arslan, E. Gedik, Implementation of hybrid nanofluid flowing in dimpled tube subjected to magnetic field, *International Communications in Heat and Mass Transfer* 134 (2022) 106032.